Eur. Phys. J. A (2018) **54**: 150
DOI 10.1140/epja/i2018-12587-1

THE EUROPEAN PHYSICAL JOURNAL A

Regular Article – Theoretical Physics

Neutron pick-up in the ^{55}Mn(d, t)^{54}Mn reaction

E.N. Cardozo[1], M.J. Ermamatov[1,2], J.L. Ferreira[1], B. Paes[1], M. Sinha[3], and J. Lubian[1,a]

[1] Instituto de Física, Universidade Federal Fluminense, 24210-340, Niterói, Rio de Janeiro, Brazil
[2] Institute of Nuclear Physics, Ulughbek, Tashkent 100214, Uzbekistan
[3] Department of Physics, Bose Institute, 93/1 Acharya Prafulla Chandra Road, Kolkata-700009, India

Received: 5 April 2018 / Revised: 6 August 2018
Published online: 17 September 2018

Communicated by P. Capel

Abstract. In this paper, we analyze the one-neutron pick-up from the ^{55}Mn target when it is bombarded by 17 MeV deuteron, by performing coupled reaction channel (CRC) calculations. Spectroscopic amplitudes for CRC calculations, and structural information such as reduced $B(E2)$ transition probabilities, quadrupole, and magnetic momenta, are obtained from shell-model calculations using the *fp-kb3* interaction. The calculated structure quantities are in good agreement with the available experimental data for both target and ejectile. Analyses of angular distributions show the relevance of microscopic information for the description of the higher excited states of ^{54}Mn.

1 Introduction

The study of transfer reactions of one or two neutrons from the projectile to the target (stripping) or vice versa (pick-up) has been a subject of recent intensive investigations [1–18]. This kind of studies is useful for extracting nuclear structure information, such as microscopic origin and nature of the ground and excited states of nuclei, paring correlations, properties of natural and un-natural parity states, etc.

Recent analyses have been mainly devoted to two-neutron transfer reactions [1,8–11,13,19]. In [8], for example, angular distributions for the ^{64}Ni(^{18}O,^{16} O)^{66}Ni transfer reactions were measured. The data were analyzed using the extreme cluster, independent coordinates model, and two-step coupled channel Born approximation (CCBA). The two-neutron transfer angular distributions have been studied in a wide mass range of targets, using (^{18}O,^{16} O) transfer reactions, with microscopic spectroscopic amplitudes and without free parameters.

In [9] a theoretical analysis has been performed for high-lying states of the ^{18}O nucleus initially with the measurement of the ^{16}O$(t,p)^{18}$O reaction at 15 MeV and further analysing new experimental cross sections for the high-lying states of the ^{18}O residual nucleus, populated in the ^{16}O(^{18}O,^{16} O)^{18}O reaction at 84 MeV. The effect of pairing correlations was shown by comparing two-step and one-step transfer reactions to the ground, as well as excited states.

In (p,t), (t,p) and (d,t) reactions, particles can be detected with high energy resolution, and theoretical calculations are not connected with complicated couplings, because of the absence of bound excited states in deuteron and triton. Nuclear reaction and structure analyses can be performed by these processes [20–28].

The proton pickup reaction, ^{27}Al$(d,{}^3$He$)^{26}$Mg [29] was studied at 25 MeV beam energy and analyzed using the zero-range distorted wave Born approximation (DWBA). The spectroscopic factor strengths for the one-proton and one-neutron pick-up reactions ^{27}Al$(d,{}^3$He$)^{26}$Mg and ^{27}Al$(d,t)^{26}$Al, were obtained from the experimental data in [30] and compared with the shell model by phenomenological USDB interaction and so-called IMSRG (in-medium similarity re-normalization group) and CCEI (coupled-cluster effective interaction).

Many (d,p) and (d,n) stripping, (d,t) and (d,α) pick-up reactions have been analyzed in [12] and in the references therein. The calculations of the stripping and pick-up contributions were performed using the DWBA and CRC formalisms. The post or prior form of distorted-wave transition amplitudes have been used for $(d,n/p)$ stripping and $(d,t/\alpha)$ pick-up reactions, where the neutron-proton effective interaction in deuteron and deuteron-neutron effective interaction in triton were assumed to have a Gaussian shape. A Woods-Saxon shape of the potential has been used for the deuteron-deuteron effective interaction.

In the case of the two-step (or sequential) two-neutron transfer reactions [8–11], intermediate partitions appear due to the one-neutron transfer. So, it is very important to verify whether the one-neutron transfer is properly accounted for in our two-neutron transfer studies. For

[a] e-mail: lubian@if.uff.br

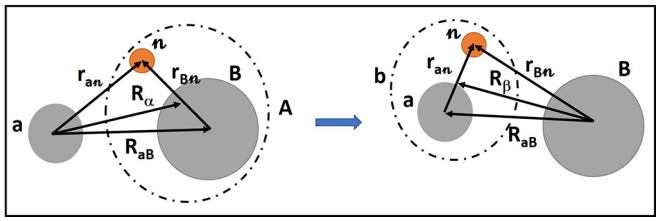

Fig. 1. (Color online) Pick-up reaction picture with corresponding relevant coordinates.

the ^{12}C(^{18}O,^{16} O)^{14}C reaction it has been confirmed for the one-neutron transfer between the intermediate and the final partition (^{13}C(^{17}O,^{16} O)^{14}C). However, for the transition between the initial and intermediate partition, this has to be checked upon experimental data. For the other systems, the validity of the one-neutron transfer results has not been checked between any of the transitions (initial-intermediate, neither intermediate-final). To verify the accuracy of our one-neutron transfer reaction calculation procedure we have selected such a system for which there are experimental data for many states because in the two-step two-neutron transfer reactions many states can be populated in the intermediate partitions.

With this purpose, we select the ^{55}Mn$(d,t)^{54}$Mn reaction in which the measurement of the angular distributions of the excited state of ^{54}Mn up to 4 MeV has been performed by Cameron *et al.* [22], where spectroscopic factors have been obtained for mixed j-particle transferred angular momentum. Besides that, the phenomenological global potentials were used for deuteron and triton effective interactions, as proposed in refs. [31,32] to perform DWBA calculation. In these works, very low spectroscopic factors were observed for high j-transfer and also for higher excited states.

In this context, we have studied the ^{55}Mn$(d,t)^{54}$Mn reaction within CRC formalism for the all possible mixed transitions by considering a full microscopic calculation. The spectroscopic and structural characteristics are obtained by shell model calculations with the Kuo-Brown *fp-kb3* interaction [33], which has shown good results in $A > 50$ region. The Sao Paulo potential has been used as the optical potential which allows describing reactions without performing any fitting of the optical potential parameters. Moreover, previously measured elastic scattering data of $d + ^{55}$Mn reaction have been compared with the estimation of the coupled channel calculations using the Sao Paulo potential.

In sect. 2, the ^{55}Mn$(d,t)^{54}$Mn one-neutron stripping reaction is analysed within the CRC formalism and the results are compared with the DWBA approach. In sect. 3, the conclusions are drawn.

2 Results and discussion

2.1 Coupled reaction channel calculations

In fig. 1, a simplified reaction process is sketched, where the projectile (a deuteron) is impinged on the target, composed by core plus a valence particle (^{54}Mn + n), and picks up this valence neutron from it. After the collision, the picked neutron leave the target bound state and is bound onto the deuteron, so that, the final partition may be represented by the $t + ^{54}$Mn system. Supposing that the target and residual nuclei remained in ground states during the transfer process, the transition matrix element for this reaction can be written, in prior representation, as

$$T_{\alpha\beta} = \left\langle \Psi_\beta^{(-)} | U(\mathbf{R}_{aB}) + v(\mathbf{r}_{an}) - U(\mathbf{R}_\alpha) | \Psi_\alpha^{(+)} \right\rangle, \quad (1)$$

with $\Psi_\beta^{(-)} \to \Psi_\beta^{(-)}(\mathbf{R}_\beta, \mathbf{r}'_{an}, \mathbf{r}'_{Bn})$, is the time-reversed total wave function of the $t+^{54}$Mn outgoing partition, while $\Psi_\alpha^{(+)} \to \Psi_\alpha^{(+)}(\mathbf{R}_\alpha, \mathbf{r}_{an}, \mathbf{r}_{Bn})$ is the total wave function for the $d + ^{55}$Mn partition. The superscript $(+)$ and $(-)$ are related to the outgoing and ingoing waves, respectively. Both, $U(\mathbf{R}_{aB})$ and $U(\mathbf{R}_\alpha)$ potentials, are effective and complex interactions describing the elastics scattering of the $d + ^{54}$Mn and $d + ^{55}$Mn systems, respectively. Conversely, the $v(\mathbf{r}_{an})$ potential is a real interaction used to bind the valence particle to the core. The labels α and β stand for all the quantum numbers necessary to specify the state in each partition. Thus, the transfer differential cross section can be calculated by

$$\frac{\mathrm{d}\sigma_{\alpha\beta}}{\mathrm{d}\Omega} = \frac{\mu_\alpha \mu_\beta}{(2\pi\hbar^2)^2} \frac{k_\beta}{k_\alpha} \frac{1}{(2I_a+1)(2I_A+1)} |T_{\alpha\beta}|^2, \quad (2)$$

where μ_α and μ_β correspond to the reduced mass of the ingoing and outgoing partitions, respectively; k_α and k_β are their corresponding wave numbers; I_a and I_A are the spins of the projectile and target, respectively.

To access to the collective states of the target, the Coulomb and nuclear parts of the optical potential can be deformed. The deformation of the potentials is usually accounted in terms of the deformation length parameter (δ_λ). For small deformations, the deformed nuclear interaction can be written as

$$V_\lambda = -\frac{\delta_\lambda}{\sqrt{4\pi}} \frac{\mathrm{d}U(R)}{\mathrm{d}R}, \quad (3)$$

where $U(R)$ is the nuclear part of the optical potential.

For the Coulomb deformations, one can relate the reduced matrix element $\langle I' || E_\lambda || I \rangle$, concerning the transition from the I initial state to the I' final state, to the reduced electric transition probability of multipolarity λ ($B(E_\lambda; I \longrightarrow I')$), so that the Coulomb reduced matrix element can be written as

$$M(E_\lambda) = \pm\sqrt{(2I+1)B(E_\lambda; I \longrightarrow I')}. \quad (4)$$

In this way, taking the reduced transition probability from the literature, one gets a model independent reduced matrix elements [34].

Here, angular distributions of the one-neutron transfer pick-up in the ^{55}Mn + d reaction have been obtained by performing prior exact finite range within the CRC framework using the Fresco code [35]. Nonorthogonality

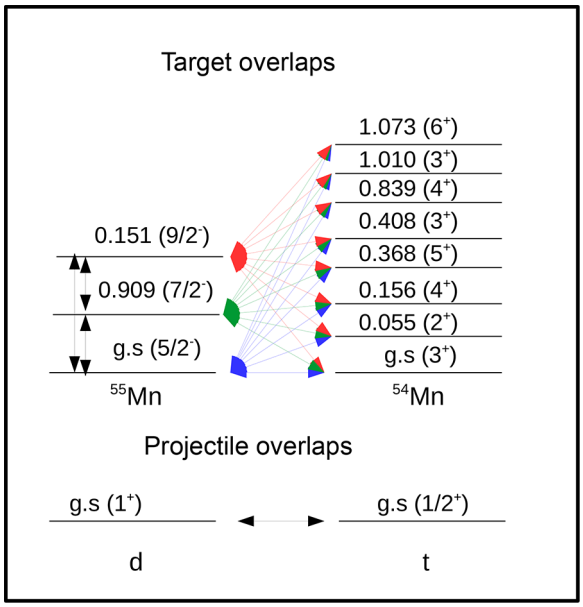

Fig. 2. (Color online) Coupling scheme used in the calculations.

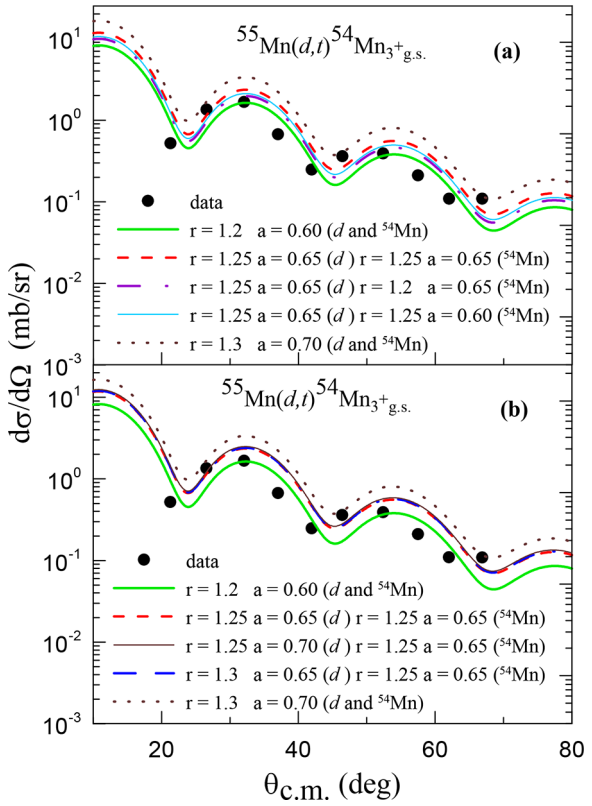

Fig. 3. (Color online) Comparison of the angular distributions of neutron pick-up calculations with the experimental data for the ^{55}Mn$(d,t)^{54}$Mn reaction to the ^{54}Mn ground state when the radius and diffuseness of the potentials that bound the valence particle to the core are varied. (see text for details).

corrections and full complex remnant terms were considered in the coupled-channel equations [34,36]. For the real and imaginary parts of the optical potential, the Sao Paulo double folding potential [37] was used. Experimental data are reported in ref. [22], where beams of 17 MeV deuterons from the McMaster FN tandem Van de Graaff accelerator were used for performing ^{55}Mn$(d,t)^{54}$Mn reaction.

In the entrance partition, a strength factor of 0.6 was used in the imaginary part of the optical potential because this factor accounts for the missing couplings to dissipative processes which are not explicitly considered in the calculations, as the coupling to continuum states [38]. In the outgoing partition, the strength factor for the imaginary part of the optical potential is set equal to 0.78, since no couplings are considered explicitly. This procedure has been shown to be suitable for describing the elastic scattering cross sections for many systems [39]. Also, the spin-orbital potential was introduced in the entrance partition with $V_{ls} = -6.2$ MeV, $r_{ls} = 1.01$ fm and $a_{ls} = 0.75$ fm parameters. The coupling schemes of projectile and target overlaps needed for one-neutron transfer reaction calculations are sketched in fig. 2.

To generate the single-particle wave functions, Woods-Saxon form-factors were used. The reduced radii and diffuseness were set to 1.25 fm and 0.65 fm for both deuteron and ^{54}Mn. The depths of the Woods-Saxon potentials were varied to fit the experimental one-neutron binding energies. Then, the reduced radii and diffuseness were varied for both nuclei, to check the sensitivity of the absolute value of the derived angular distributions to these parameters. The reduced radii were varied from 1.2 fm to 1.3 fm, while the diffuseness from 0.6 fm to 0.7 fm, which we are considering as lower and upper limit for both parameters. From fig. 3, one observes the effect of the variation of these parameters of the potential binding the neutron to the deuteron (a) and ^{54}Mn (b), on the angular distribution of the $t + ^{54}$Mn(3^+_1) channel. One can notice that the variation of the angular distribution is not negligible, but at the same time is not so strong. At most, the cross section has been increased by a factor 2 when the lower and upper limits for the geometric parameters are taken.

The same result was obtained for the other channels in which the residual ^{54}Mn remains in excited states. We showed the results for the ground state, as an example.

As mentioned above, the Sao Paulo potential will be used as an optical potential in both entrance and final partitions. To show that this potential is suitable for describing the elastic scattering angular distribution we look in literature for experimental data. In ref. [40] the elastic scattering angular distribution is available for the ^{55}Mn$(d,d)^{55}$Mn reaction at a beam energy of 46 MeV, well above the Coulomb barrier. Firstly, we performed a one-channel calculation using the Sao Paulo potential as an optical potential for this beam energy with standard normalization strength 1.0 and 0.78 for the real and imaginary parts, respectively [39]. Next, inelastic and transfer channels are included in the calculations to check the influence of them on the elastic channel. In this case, the coefficient of the imaginary part of the optical potential was decreased to 0.6 because couplings were included explicitly. The comparison of the calculation with these experimental data is shown in fig. 4. One can see that the

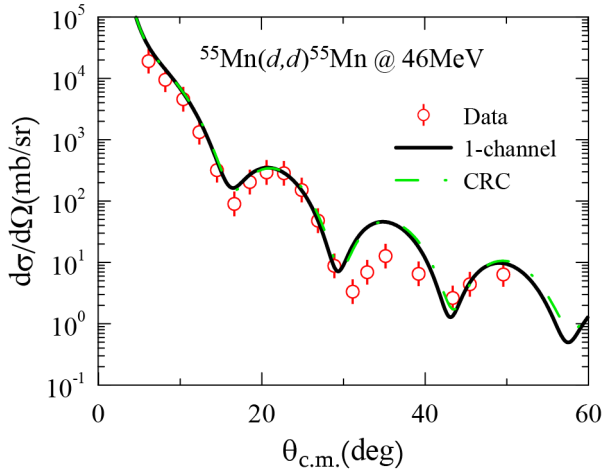

Fig. 4. (Color online) Comparison of the calculated elastic scattering angular distribution in ^{55}Mn$(d,d)^{55}$Mn at 46 MeV beam energy with the experimental data [40].

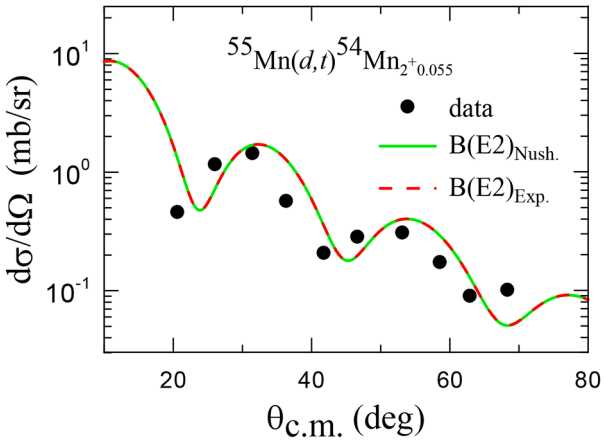

Fig. 5. (Color online) Comparison of the theoretical angular distribution with the experimental data for the ^{55}Mn$(d,t)^{54}$Mn reaction for the ^{54}Mn in the 2^+ state. The dashed red lines correspond to the CRC calculations considering the experimental electric reduced transition probabilities, while the full green lines stands for the electric reduced transition probabilities obtained from the shell model calculations.

agreement with the experimental data is quite good taking into account that there is no fit procedure in these calculations, even after the inclusion of the inelastic and transfer channels. In fact, the influence of these channels is very small. This allows us to use the Sao Paulo potential at 17 MeV also, with high confidence.

Spectroscopic amplitudes for the one-neutron transfer overlaps were obtained performing shell-model calculations with NuShellX code [41]. The *fp* model space and effective interaction *kb3* [33] have been used. In this model space, the ^{40}Ca nucleus is considered as a closed core, and the $1f_{7/2}$, $2p_{3/2}$, $1f_{5/2}$, $2p_{1/2}$ are taken as valence subspace for the neutrons and protons.

For the projectile overlap, the spectroscopic amplitude was set to 1.22 where this value was obtained by microscopic calculation reported in ref. [42]. The spectroscopic amplitudes used in the one-neutron transfer calculation relative to the target overlaps are shown in table 1, where $\mathbf{nl_j}$ are the principal quantum numbers, the orbital and the total angular momenta of the single neutron.

The coupling matrix elements concerning the inelastic excitations of the target (see fig. 2) were derived by considering the reduced electric quadrupole transition probabilities $B(E2)$, which have been deduced from our shell model calculations. In fact, we also performed calculations using the experimental values from ref. [1], and the results for the transfer cross sections were almost the same as shown in fig. 5 for the ^{55}Mn$(d,d)^{55}$Mn$_{0.055(2^+)}$. The results for the other final channels were exactly the same. To complete the structural picture, the $B(M1)$ and quadrupole momenta for the ^{54,55}Mn, as well as the reduced $B(E2)$ obtained from shell model calculations are compared with experimental data in table 2. As can be seen from table 2 these properties are described by the shell model reasonably well.

As is seen from table 1, the neutron pick-up is allowed from all $2p_{1/2}$, $2p_{3/2}$, $1f_{5/2}$ and $1f_{7/2}$ orbitals by angular momentum conservation when the ^{54}Mn nucleus is in the ground state, and ^{55}Mn is in the ground and 0.126 MeV $(7/2^-)$ states. In this case, the probabilities of neutron pick-up from different orbitals are similar, the most probable orbital being $2p_{3/2}$. The transfer from $2p_{1/2}$ orbital is not allowed by angular momentum conservation when ^{55}Mn is in 0.984 MeV $(9/2^-)$ state, where now $1f_{5/2}$ become more important. In fig. 6, the theoretical and experimental angular distributions are shown when the residual nucleus are in g.s. (3^+), 0.055 MeV (2^+), 0.156 MeV (4^+), 0.358 MeV (5^+), 0.408 MeV (3^+), 0.809 MeV (4^+), 1.010 MeV (3^+) and 1.073 MeV (6^+) states. From fig. 6, one can see that the order of magnitude and shape of the angular distribution in the g.s. of the residual nucleus are described quite well. There is a small difference in the phases of the experimental and calculated angular distribution oscillations.

For the 0.055 MeV (2^+) and 0.156 MeV (4^+) states of ^{54}Mn, in which as is seen from table 1, again coupling with g.s. $(5/2^-)$ of ^{55}Mn is important and the major contribution is from $2p_{3/2}$. In these two states the quality of the agreement of the order, phase, and amplitudes of the angular distribution oscillations are very similar to that when both nuclei were in the ground states, but as the excitation energy of the residual nuclei becomes higher, the cross section of these states becomes smaller. Apparently, this is connected with the fact that the values of the spectroscopic amplitudes corresponding to these target overlaps are considerably smaller than the ones related to the two states mentioned above (see table 1).

For the coupling of the 0.368 MeV (5^+) state of ^{54}Mn with the g.s. of ^{55}Mn, only $1f_{5/2}$ and $1f_{7/2}$ orbitals are allowed, with more probability of the $1f_{7/2}$ orbital. In the couplings of this state with the other two 0.126 MeV $(7/2^-)$ and 0.984 MeV $(9/2^-)$ states of ^{54}Mn still, the main contribution comes from $2p_{3/2}$. The calculated angular distribution describes reasonably well the experimental

Table 1. One-neutron spectroscopic amplitudes (SA).

One-neutron amplitudes			
Initial state	$\mathbf{nl_j}$	Final state	SA
$^{55}\mathrm{Mn}_{\mathrm{g.s.}}(5/2^-)$	$2p_{1/2}$	$^{54}\mathrm{Mn}_{\mathrm{g.s.}}(3^+)$	−0.418
	$2p_{3/2}$		−0.647
	$1f_{5/2}$		0.168
	$1f_{7/2}$		−0.0971
	$2p_{1/2}$	$^{54}\mathrm{Mn}_{0.055}(2^+)$	0.423
	$2p_{3/2}$		−0.524
	$1f_{5/2}$		−0.149
	$1f_{7/2}$		−0.040
	$2p_{3/2}$	$^{54}\mathrm{Mn}_{0.156}(4^+)$	−0.426
	$1f_{5/2}$		0.046
	$1f_{7/2}$		−0.184
	$1f_{5/2}$	$^{54}\mathrm{Mn}_{0.368}(5^+)$	−0.080
	$1f_{7/2}$		0.174
	$2p_{1/2}$	$^{54}\mathrm{Mn}_{0.408}(3^+)$	0.198
	$2p_{3/2}$		−0.356
	$1f_{5/2}$		−0.215
	$1f_{7/2}$		−0.138
	$2p_{3/2}$	$^{54}\mathrm{Mn}_{0.839}(4^+)$	0.142
	$1f_{5/2}$		−0.262
	$1f_{7/2}$		−0.004
	$2p_{1/2}$	$^{54}\mathrm{Mn}_{1.010}(3^+)$	−0.131
	$2p_{3/2}$		−0.023
	$1f_{5/2}$		0.149
	$1f_{7/2}$		−0.019
	$1f_{7/2}$	$^{54}\mathrm{Mn}_{1.073}(6^+)$	1.051
$^{55}\mathrm{Mn}_{0.126}(7/2^-)$	$2p_{1/2}$	$^{54}\mathrm{Mn}_{\mathrm{g.s.}}(3^+)$	0.243
	$2p_{3/2}$		0.438
	$1f_{5/2}$		−0.202
	$1f_{7/2}$		0.131
	$2p_{3/2}$	$^{54}\mathrm{Mn}_{0.055}(2^+)$	−0.449
	$1f_{5/2}$		−0.203
	$1f_{7/2}$		−0.121
	$2p_{1/2}$	$^{54}\mathrm{Mn}_{0.156}(4^+)$	0.118
	$2p_{3/2}$		0.600
	$1f_{5/2}$		0.087
	$1f_{7/2}$		−0.054
	$2p_{3/2}$	$^{54}\mathrm{Mn}_{0.368}(5^+)$	0.542
	$1f_{5/2}$		−0.113
	$1f_{7/2}$		0.087
	$2p_{1/2}$	$^{54}\mathrm{Mn}_{0.408}(3^+)$	0.318
	$2p_{3/2}$		−0.307
	$1f_{5/2}$		0.033
	$1f_{7/2}$		0.062
	$2p_{1/2}$	$^{54}\mathrm{Mn}_{0.839}(4^+)$	−0.393
	$2p_{3/2}$		0.113
	$1f_{5/2}$		0.091
	$1f_{7/2}$		0.008
	$2p_{1/2}$	$^{54}\mathrm{Mn}_{1.010}(3^+)$	−0.079
	$2p_{3/2}$		−0.484
	$1f_{5/2}$		−0.149
	$1f_{7/2}$		−0.048
	$1f_{5/2}$	$^{54}\mathrm{Mn}_{1.073}(6^+)$	0.027
	$1f_{7/2}$		−0.656

Table 1. Continued.

One-neutron amplitudes			
Initial state	$\mathbf{nl_j}$	Final state	SA
$^{55}\mathrm{Mn}_{0.984}(9/2^-)$	$2p_{3/2}$	$^{54}\mathrm{Mn}_{\mathrm{g.s.}}(3^+)$	−0.148
	$1f_{5/2}$		0.254
	$1f_{7/2}$		−0.133
	$1f_{5/2}$	$^{54}\mathrm{Mn}_{0.055}(2^+)$	0.161
	$1f_{7/2}$		0.107
	$2p_{1/2}$	$^{54}\mathrm{Mn}_{0.156}(4^+)$	−0.500
	$2p_{3/2}$		−0.317
	$1f_{5/2}$		0.089
	$1f_{7/2}$		−0.107
	$2p_{1/2}$	$^{54}\mathrm{Mn}_{0.368}(5^+)$	0.275
	$2p_{3/2}$		0.383
	$1f_{5/2}$		0.117
	$1f_{7/2}$		−0.113
	$2p_{3/2}$	$^{54}\mathrm{Mn}_{0.408}(3^+)$	0.585
	$1f_{5/2}$		0.173
	$1f_{7/2}$		−0.008
	$2p_{1/2}$	$^{54}\mathrm{Mn}_{0.839}(4^+)$	−0.091
	$2p_{3/2}$		0.418
	$1f_{5/2}$		−0.219
	$1f_{7/2}$		−0.064
	$2p_{3/2}$	$^{54}\mathrm{Mn}_{1.010}(3^+)$	−0.121
	$1f_{5/2}$		0.014
	$1f_{7/2}$		−0.057
	$2p_{3/2}$	$^{54}\mathrm{Mn}_{1.073}(6^+)$	−0.016
	$1f_{5/2}$		−0.028
	$1f_{7/2}$		0.301

data, and the amplitudes of the oscillations are decreased as compared to the ones of the states mentioned above.

The contributions from the different spherical orbitals to the angular distributions, when the residual nucleus is in the 0.408 MeV (3^+) state, are similar to those of the first 3^+ state, hence the similarity in the shape and amplitude of oscillation of the angular distribution.

A similar comparison of spectroscopic amplitudes between the couplings of the 0.839 MeV (4^+) state of ^{54}Mn and the ^{55}Mn states with previous 4^+ state shows a difference in the probability distribution among different orbitals. This is also seen in the angular distributions of this state from fig. 6, *i.e.*, the oscillations in the angular distribution here are smaller than in the previous 4^+ state.

The same regularity is seen in the angular distribution of 1.010 MeV (3^+) state. The spectroscopic amplitudes are distributed different way among the orbitals as compared to the previous 3^+ states, *i.e.*, such a way that oscillations of the angular distribution of the present 3^+ state are smaller than those of the previous 3^+ states.

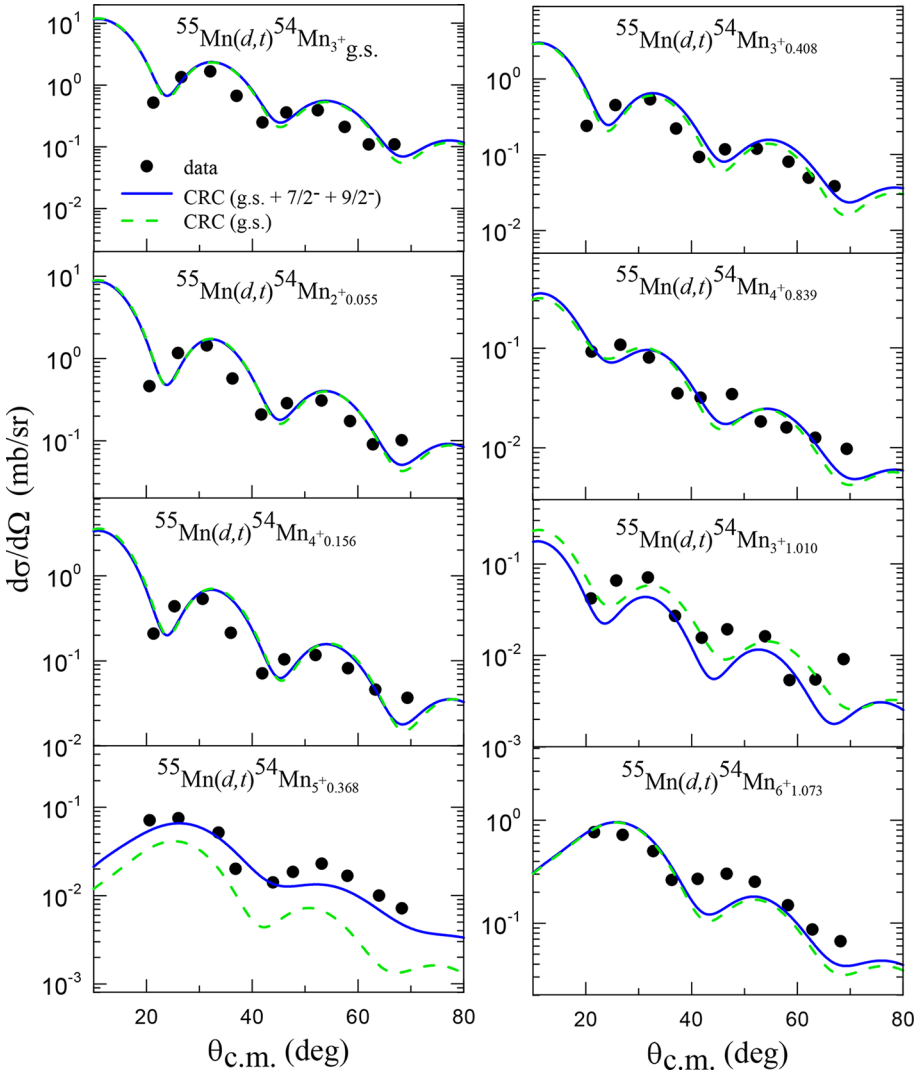

Fig. 6. (Color online) Comparison of CRC theoretical results, switching on and off the overlaps including the ^{55}Mn excited states, with the experimental data. The full blue lines correspond to CRC calculations taking into account the transfer from the excited states of the ^{55}Mn. The dashed green lines correspond to the CRC (or DWBA) calculations where only the ground state of the ^{55}Mn nucleus is considered in the coupling scheme.

It is seen from table 1 for 1.073 MeV (6^+) state the spectroscopic amplitude from $1f_{7/2}$ is much higher than those from other orbitals. So, this orbital is relevant for the agreement of the theoretical cross section with the experimental angular distribution of this state (see fig. 6).

For all states, the phases in the oscillations of the angular distributions in the calculation are slightly shifted as compared to the experiment. Nevertheless, the general agreement between the theoretical results and the experimental data is quite good. This allows us to be confident about our parameter-free procedure used in the calculation of one-neutron transfer not only for the first excited states but also for higher states. Of course, the success of this procedure strongly depend on the correct choice of the interaction and model space determined by the accurate description of the nuclear structure properties of the involved nuclei.

2.2 Comparison between DWBA and CRC calculations

Finally, we performed DWBA calculation for this system to clarify the effect of the high-order couplings on this transfer reaction. Our DWBA calculations show that the high-order couplings are not very significant to describe the angular distribution of most of the states analised in the present work, contrary to what happened in the two-neutron transfer reaction studied by us in a previous work [11]. This means that the spectroscopic amplitudes could be determined by fitting the angular distributions by means of DWBA calculations using a proper optical potential that describes the elastic scattering. However, this is true when only one single-particle component is allowed for the overlap of the initial and final states. In microscopic calculations, as we are doing here, there is no need to worry about this, since in describing the structure

Table 2. Comparison of the $B(M1)$ and $B(E2)$ transition probabilities, calculated within shell model with *fp-kb3* interaction, of ^{54,55}Mn isotopes with experimental data [43].

^{54}Mn			
	I^π	Expt.	*fp-kb3*
Q [eb]	3_1^+	+0.37(3)	+0.35
μ [μ_N]	3_1^+	3.2819(13)	2.767
	$I_i^\pi \to I_f^\pi$	Expt.	*fp-kb3*
$B(M1)$ [W.u.]	$2_1^+ \to 3_1^+$	2.3(10)	0.92
	$4_1^+ \to 3_1^+$	0.0307(25)	0.0171
	$5_1^+ \to 4_1^+$	0.33(4)	0.35
	$3_2^+ \to 2_1^+$	0.026(5)	0.023
	$3_2^+ \to 4_1^+$	0.48(17)	0.85
	$3_2^+ \to 3_1^+$	0.051(18)	0.073
	$4_2^+ \to 5_1^+$	0.19(4)	0.39
$B(E2)$ [W.u.]	$4_1^+ \to 3_1^+$	2.4(9)	9.77
	$5_1^+ \to 3_1^+$	8.9(11)	5.84
	$3_2^+ \to 2_1^+$	14(8)	16.81
^{55}Mn			
	I^π	Expt.	*fp-kb3*
Q [eb]	$5/2_1^-$	+0.33(1)	+0.36
μ [μ_N]	$5/2_1^-$	3.4532(13)	3.371
$B(M1)$ [W.u.]	$7/2_1^- \to 5/2_1^-$	0.0417(13)	0.034
	$9/2_1^- \to 7/2_1^-$	0.110(13)	0.056
	$11/2_1^- \to 9/2_1^-$	0.171(22)	0.143
	$3/2_1^- \to 5/2_1^-$	0.092(20)	0.085
	$7/2_2^- \to 7/2_1^-$	0.12(5)	0.145
	$7/2_2^- \to 5/2_1^-$	0.17(5)	0.156
$B(E2)$ [W.u.]	$7/2_1^- \to 5/2_1^-$	14.7(23)	27.51
	$9/2_1^- \to 5/2_1^-$	8.8(11)	7.88
	$9/2_1^- \to 7/2_1^-$	23(3)	17.54
	$11/2_1^- \to 9/2_1^-$	3.(5)	14.75
	$11/2_1^- \to 7/2_1^-$	14.4(15)	14.54
	$1/2_1^- \to 5/2_1^-$	11.6(10)	4.43
	$3/2_1^- \to 5/2_1^-$	3.3(21)	1.79
	$7/2_2^- \to 5/2_1^-$	2.6(8)	3.44
	$7/2_2^- \to 7/2_1^-$	< 1	0.21

of involved nuclei, the possible couplings appear naturally, according to the model space chosen.

As already mentioned in sect. 2.1, we are using the spectroscopic amplitudes derived by performing shell model calculations where the *fp-kb3* phenomenological interaction was used. This interaction is a modified version of the one used in ref. [44] (*fp-kb*). In ref. [22] Cameron *et al.* compared the spectroscopic factors derived using the (*fp-kb*) interaction with the ones obtained from DWBA fits to the experimental angular distributions. Indeed, the spectroscopic factors obtained using the *fp-kb3* interaction are close to those obtained in both refs. [44,45] by using DWBA approach and the *fp-kb* interaction, as one can observe from table 3. As the spectroscopic factors are very similar, one should expect that the transfer angular distributions would be similar too.

Table 3. Comparison among the one-neutron spectroscopic factors used in refs. [22,45] and the derived in the present work.

One-neutron amplitudes					
Initial state	$\mathbf{nl_j}$	Final State	SF *pf-kb3*	SF [22,45] *pf-kb*	SF [22] DWBA
^{55}Mn$(5/2_1^-)$	$2p_{1/2}$	^{54}Mn(3_1^+)	0.175	0.19	0.15
	$2p_{3/2}$		0.419	0.48	0.33
	$1f_{5/2}$		0.028	0.09	–
	$1f_{7/2}$		0.009	–	–
	$2p_{1/2}$	^{54}Mn(2_1^+)	0.179	0.19	0.14
	$2p_{3/2}$		0.275	0.30	0.26
	$1f_{5/2}$		0.022	0.05	–
	$1f_{7/2}$		0.002	–	–
	$2p_{3/2}$	^{54}Mn(4_1^+)	0.181	0.200	0.150
	$1f_{5/2}$		0.002	0.010	–
	$1f_{7/2}$		0.034	–	–
	$1f_{5/2}$	^{54}Mn(5_1^+)	0.006	0.002	0.060
	$1f_{7/2}$		0.030	–	–
	$2p_{1/2}$	^{54}Mn(3_2^+)	0.039	0.050	0.060
	$2p_{3/2}$		0.127	0.130	0.08
	$1f_{5/2}$		0.046	0.090	(0.120)
	$1f_{7/2}$		0.019	–	–
	$2p_{3/2}$	^{54}Mn(4_2^+)	0.020	0.026	(0.010)
	$1f_{5/2}$		0.069	0.130	0.120
	$1f_{7/2}$		0.000	–	–
	$2p_{1/2}$	^{54}Mn(3_3^+)	0.017	0.030	0.020
	$2p_{3/2}$		0.001	0.001	0.000
	$1f_{5/2}$		0.022	0.100	(0.040)
	$1f_{7/2}$		0.000	–	–
	$1f_{7/2}$	^{54}Mn(6_1^+)	1.105	1.240	0.900

In fig. 7, a comparison among the theoretical results using spectroscopic factors given in table 3 and experimental data is shown. A quite good agreement among the three theoretical angular distributions and with the experimental data is observed, as expected. The most relevant difference between the results using *pf-kb3* and *pf-kb* interactions is observed for the t+^{54}Mn(5_1^+) channel.The reason for this difference lays in the fact that the spectroscopic factor of the target overlap $\langle ^{54}\text{Mn}(5_1^+)|^{55}\text{Mn}(3_1^+)\rangle$ involving the Mn(5_1^+) state is considerably different in both interactions (see table 3).

Besides, to check the effect of the transfer from the ^{55}Mn$(7/2_1^-)$ and ^{55}Mn$(9/2_1^-)$ excited states of the target on the transfer angular distributions we performed a comparison of the CRC calculations switching on and off

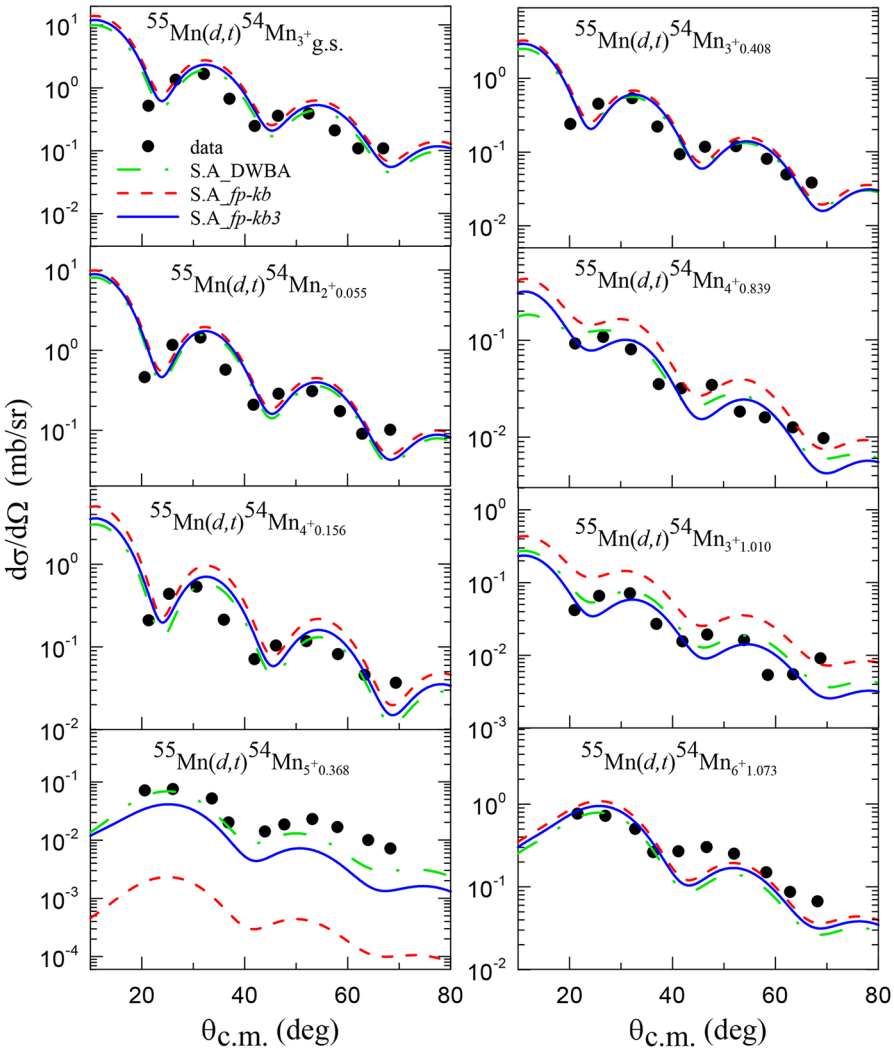

Fig. 7. (Color online) The dot-dashed green lines correspond to the transfer cross section calculations using the spectroscopic factors fitted by the DWBA method [22]; dashed red lines correspond to the results using and shell model spectroscopic factors of ref. [44]; the full blue lines are related to the DWBA results by using the microscopic spectroscopic factors obtained with the *pf-kb3* interaction (used also in our CRC calculations in the present work).

the overlaps including these states. Indeed, as can be seen from fig. 6, the couplings to the inelastic states of the target are relevant to describe the angular distribution of the t+^{54}Mn(5_1^+) and t+^{54}Mn(3_3^+) channels. We would like to emphasize that the results of CRC calculations switching off the overlaps including the excited states of the target are almost identical to the DWBA results using the same model space (shown in fig. 7 by a full blue line).

Moreover, although our description of the experimental data is not perfect, we have no free parameters in our optical potential, once we are using a double folding potential. Thus, even though the DWBA method describes the data by fitting both optical potential and spectroscopic factors, it can not predict the relevance of the transfer from excited states on the transfer differential cross sections. In this work, we have shown that only including the couplings with inelastic states we could describe the angular distributions for some channels by performing a full microscopic transfer calculation. Also, from table 3 one can observe, for example, that to describe the angular distribution of the t+^{54}Mn(5_1^+) channel, the DWBA fit provides a spectroscopic factor that is twice the one derived from microscopic calculations for the $\langle ^{54}\mathrm{Mn}(5_1^+)|^{55}\mathrm{Mn}(3_1^+)\rangle$ overlap.

3 Conclusion

The neutron pick-up in the $^{55}\mathrm{Mn}(d,t)^{54}\mathrm{Mn}$ reaction has been studied within CRC formalism by using a fixed systematics of potential parameters. The structure information obtained by shell model calculation with *fp-kb3* interaction describes well the order of magnitude, oscillation and shape of angular distributions when ^{54}Mn is in the ground, and several excited states. This allows us to be confident in our parameter-free description of the

one-neutron transfer reactions to the ground and excited states. We emphasize that although in our calculations there are some parameters, like the strength coefficients of the imaginary parts of the optical potentials in different participations, they are taken from systematics and they are not changed to fit the experimental data.

A comparison of the results from DWBA and CRC calculations, including transfer from excited states of the target, showed that, for some states, the effect of the transfer from excited states might be relevant. In this case, the spectroscopic factors (or amplitudes) derived from DWBA fits are overestimated and might not reveal the real structure of the wave function of these states.

Brazilian authors acknowledge the partial support from CNPq, FAPERJ, and CAPES and from INCT-FNA (Instituto Nacional de Ciência e Tecnologia- Física Nuclear e Aplicações), research project No. 464898/2014-5. MJE's work is supported by a grant from CNPq-Brazil (Process No. 165371/2015-3) and grant of the Uzbekistan National Agency of Science and Technology (OT-F2-25). MS thanks ISRO for the financial support under grant no. ISRO/RES/2/378/15-16.

References

1. M. Cavallaro, F. Cappuzzello, M. Bondì, D. Carbone, V.N. Garcia, A. Gargano, S.M. Lenzi, J. Lubian, C. Agodi, F. Azaiez, M. De Napoli, A. Foti, S. Franchoo, R. Linares, D. Nicolosi, M. Niikura, J.A. Scarpaci, S. Tropea, Phys. Rev. C **88**, 054601 (2013).
2. F. Cappuzzello, D. Carbone, M. Cavallaro, A. Cunsolo, *Magnets: Types, Uses, and Safety* (Nova Science Publishers, New York, 2011).
3. F. Cappuzzello, M. Cavallaro, A. Cunsolo, A. Foti, D. Carbone, S. Orrigo, M. Rodrigues, Nucl. Instrum. Methods Phys. Res. Sect. A **621**, 419 (2010).
4. F. Cappuzzello, C. Rea, A. Bonaccorso, M. Bondì, D. Carbone, M. Cavallaro, A. Cunsolo, A. Foti, S. Orrigo, M. Rodrigues, G. Taranto, Phys. Lett. B **711**, 347 (2012).
5. D. Carbone, Eur. Phys. J. Plus **130**, 143 (2015).
6. D. Carbone, M. Bondì, A. Bonaccorso, C. Agodi, F. Cappuzzello, M. Cavallaro, R.J. Charity, A. Cunsolo, M. De Napoli, A. Foti, Phys. Rev. C **90**, 064621 (2014).
7. D. Carbone, F. Cappuzzello, M. Cavallaro, Eur. Phys. J. A **48**, 60 (2012).
8. B. Paes, G. Santagati, R.M. Vsevolodovna, F. Cappuzzello, D. Carbone, E.N. Cardozo, M. Cavallaro, H. García-Tecocoatzi, A. Gargano, J.L. Ferreira, S.M. Lenzi, R. Linares, E. Santopinto, A. Vitturi, J. Lubian, Phys. Rev. C **96**, 044612 (2017).
9. M.J. Ermamatov, R. Linares, J. Lubian, J.L. Ferreira, F. Cappuzzello, D. Carbone, M. Cavallaro, M. Cubero, P.N. de Faria, A. Foti, G. Santagati, V.A.B. Zagatto, Phys. Rev. C **96**, 044603 (2017).
10. D. Carbone, J.L. Ferreira, F. Cappuzzello, J. Lubian, C. Agodi, M. Cavallaro, A. Foti, A. Gargano, S.M. Lenzi, R. Linares, G. Santagati, Phys. Rev. C **95**, 034603 (2017).
11. M.J. Ermamatov, F. Cappuzzello, J. Lubian, M. Cubero, C. Agodi, D. Carbone, M. Cavallaro, J.L. Ferreira, A. Foti, V.N. Garcia, A. Gargano, J.A. Lay, S.M. Lenzi, R. Linares, G. Santagati, A. Vitturi, Phys. Rev. C **94**, 024610 (2016).
12. M. Avrigeanu, E. Šimečková, U. Fischer, J. Mrázek, J. Novak, M. Štefánik, C. Costache, V. Avrigeanu, Phys. Rev. C **94**, 014606 (2016).
13. A. Parmar, Sonika, B. Roy, V. Jha, U. Pal, T. Sinha, S. Pandit, V. Parkar, K. Ramachandran, K. Mahata, S. Santra, A. Mohanty, Nucl. Phys. A **940**, 167 (2015).
14. G. Potel, A. Idini, F. Barranco, E. Vigezzi, R.A. Broglia, Rep. Prog. Phys. **76**, 106301 (2013).
15. W. von Oertzen, A. Vitturi, Rep. Prog. Phys. **64**, 1247 (2001).
16. G.L. Zhang, G.X. Zhang, S.P. Hu, Y.J. Yao, J.B. Xiang, H.Q. Zhang, J. Lubian, J.L. Ferreira, B. Paes, E.N. Cardozo, H.B. Sun, J.J. Valiente-Dobón, D. Testov, A. Goasduff, P.R. John, M. Siciliano, F. Galtarossa, R. Francesco, D. Mengoni, D. Bazzacco, E.T. Li, X. Hao, W.W. Qu, Phys. Rev. C **97**, 014611 (2018).
17. S.P. Hu, G.L. Zhang, J.C. Yang, H.Q. Zhang, P.R.S. Gomes, J. Lubian, J.L. Ferreira, X.G. Wu, J. Zhong, C.Y. He, Y. Zheng, C.B. Li, G.S. Li, W.W. Qu, F. Wang, L. Zheng, L. Yu, Q.M. Chen, P.W. Luo, H.W. Li, Y.H. Wu, W.K. Zhou, B.J. Zhu, H.B. Sun, Phys. Rev. C **93**, 014621 (2016).
18. M. Fisichella, A.C. Shotter, P. Figuera, J. Lubian, A. Di Pietro, J.P. Fernandez-Garcia, J.L. Ferreira, M. Lattuada, P. Lotti, A. Musumarra, M.G. Pellegriti, C. Ruiz, V. Scuderi, E. Strano, D. Torresi, M. Zadro, Phys. Rev. C **95**, 034617 (2017).
19. F. Cappuzzello, J. Lubian, J.R.B. Oliveira, C. Agodi, M. Bond, D. Carbone, M. Cavallaro, L.C. Chamon, A. Cunsolo, M. De Napoli, A. Foti, V. Nunes Garcia, L.R. Gasques, P.R.S. Gomes, R. Linares, D. Nicolosi, B. Paes, S. Tropea, EPJ Web of Conferences **66**, 03067 (2014).
20. M.A. Rahman, M.S. Chowdhury, Phys. Rev. C **73**, 054311 (2006).
21. M.A. Rahman, M.S. Chowdhury, Phys. Rev. C **72**, 054303 (2005).
22. J. Cameron, E. Habib, A. Pilt, R. Schubank, V. Janzen, Nucl. Phys. A **365**, 113 (1981).
23. S. Mordechai, H. Fortune, G. Moore, M. Cobern, R. Kollarits, R. Middleton, Nucl. Phys. A **301**, 463 (1978).
24. A. Baxter, S. Hinds, Nucl. Phys. A **211**, 7 (1973).
25. W. Alford, J. Cameron, E. Habib, B. Wildenthal, Nucl. Phys. A **454**, 189 (1986).
26. M.E. Cobern, L.C. Bland, H.T. Fortune, G.E. Moore, S. Mordechai, R. Middleton, Phys. Rev. C **23**, 2387 (1981).
27. T. Takemasa, H. Yoshida, Nucl. Phys. A **304**, 229 (1978).
28. M.C. Mermaz, M.A.G. Fernandes, A. Greiner, B.T. Kim, N. Lisbona, Phys. Rev. C **19**, 794 (1979).
29. V. Srivastava, C. Bhattacharya, T.K. Rana, S. Manna, S. Kundu, S. Bhattacharya, K. Banerjee, P. Roy, R. Pandey, G. Mukherjee, T.K. Ghosh, J.K. Meena, T. Roy, A. Chaudhuri, M. Sinha, A.K. Saha, M.A. Asgar, A. Dey, S. Roy, M.M. Shaikh, Phys. Rev. C **93**, 044601 (2016).
30. P.C. Srivastava, V. Kumar, Phys. Rev. C **94**, 064306 (2016).
31. J. Lohr, W. Haeberli, Nucl. Phys. A **232**, 381 (1974).
32. F.D. Becchetti, G.W. Greenlees, Phys. Rev. **182**, 1190 (1969).
33. A. Poves, A. Zuker, Phys. Rep. **70**, 235 (1981).
34. E.R. Pike, Pierre C. Sabatier (Editors), *Scattering and Inverse Scattering in Pure and Applied Science*, Vol. **1** (Academic Press, 2001).
35. I.J. Thompson, Comput. Phys. Rep. **7**, 167 (1988).

36. G.R. Satchler, *Direct Nuclear Reactions* (Clarendon Press, Oxford, Oxford University Press, NY, 1983).
37. L.C. Chamon, B.V. Carlson, L.R. Gasques, D. Pereira, C. De Conti, M.A.G. Alvarez, M.S. Hussein, M.A. Cândido Ribeiro, E.S. Rossi, C.P. Silva, Phys. Rev. C **66**, 014610 (2002).
38. D. Pereira, J. Lubian, J. Oliveira, D. de Sousa, L. Chamon, Phys. Lett. B **670**, 330 (2009).
39. L. Gasques, L. Chamon, P. Gomes, J. Lubian, Nucl. Phys. A **764**, 135 (2006).
40. R.T. Newman, R.W. Fearick, S.M. Perez, D.G. Aschman, K. Bharuth-Ram, W.A. Richter, F.D. Smit, V.M. Tshivhase, T.S. Volkwyn, Phys. Rev. C **54**, 1773 (1996).
41. NuShell for Windows and Linux, `http://www.garsington.eclipse.co.uk/`.
42. N. Burtebayev, J.T. Burtebayeva, A. Duisebayev, Zh.K. Kerimkulov, M. Nassurlla, T. Zholdybayev, S.V. Artemov, A.A. Karakhodzhayev, U.S. Salikhbayev, S.B. Sakuta, S. Kliczewski, E. Piasecki, K. Rusek, R. Siudak, A. Trzciskae, M. Woliska-Cichocka, A. Amar, Acta Phys. Pol. B **46**, 5 (2015).
43. `www.nndc.bnl.gov/ensdf`.
44. I.P. Johnstone, H.G. Benson, J. Phys. G: Nucl. Phys. **3**, 4 (1977).
45. T. Taylor, J.A. Cameron, Nucl. Phys. A **257**, 427 (1976).